WIND RESPONSE CHARACTERISTICS OF HORIZONTAL AXIS WIND TURBINES

R.W. Thresher, W.E. Holley and N. Jafarey

Mechanical Engineering Department
Oregon State University
Corvallis, OR 97331

INTRODUCTION

The dynamic response of wind turbines to turbulent wind fluctuations has generally been modeled using only changes in the streamwise wind velocity as the disturbance which causes the varying aerodynamic forces and moments. Often these wind fluctuations are thought of, and modeled, as discrete wind gusts of specified shape and duration, which occur at some average rate. In addition, these wind fluctuations usually have been assumed to act uniformly over the entire rotor disk. In terms of the designer's needs, these models are used to generate design loads and expected control system actions.

It was the objective of the work reported here, and in the companion paper [1], to take a broader look at wind turbine dynamic response to turbulence, and attempt to ascertain the features of turbulence that wind turbines are most sensitive to. A statistical description of the wind input including all three wind components and allowing linear wind gradients across the rotor disk, was used together with quasi-static aerodynamic theory and an elementary structural model involving only a few degrees of freedom. The idea was to keep the turbine model simple and show the benefits of this type of statistical wind representation before attempting to use a more complex turbine model. As far as possible, the analysis was kept in the simplest form, while still preserving key physical responses.

From the onset of this work, it was felt that the results should be validated by comparison with test measurements. Due to the three-bladed rigid rotor used on the turbine and the limited degrees of freedom, comparison with data from one of the small systems under test at Rocky Flats would provide the most realistic comparison. At this time, the experimental comparison is incomplete.

The Turbine Model

The wind turbine model is shown schematically in Figure 1. Both the rotor and the nacelle are assumed to be rigid bodies which move in unison, except for the spinning rotor. Due to tower flexibility, the nacelle and rotor are free to translate in a plane parallel to the ground and rotate about the top of the tower in pitch and yaw. The yaw angle of the rotor axis is defined by the angle, ϕ, and the pitch angle by χ. The lateral translation, U, is in the x direction, while the V translation is in the y direction along the rotor axis. The rotor spin velocity is given by $\Omega + \dot{\Psi}$, where Ω is the mean rotation rate and Ψ is some small fluctuation. For the case of a turbine with a three-bladed rigid rotor, the basic principles of Newtonian mechanics and linear, quasi-steady aerodynamics give motion equations of the form

$$M_{ij}\ddot{X}_j + C_{ij}\dot{X}_j + K_{ij}X_j = F_{ij}V_j \qquad (1)$$

where M_{ij}, C_{ij}, K_{ij} and F_{ij} are the turbine system inertia, damping, stiffness and wind input coefficients. The five displacement coordinates already described are X_j, while the wind inputs are V_j.

The Tower

The wind turbine tower was modeled as a single finite element within which the tower displacements were expressed in terms of interpolating polynomials and the displacements at the top of the tower. Then the tower deformation, v(z,t), about one bending axis was written in the form

$$v(z,t) = P_V(z)V(t) + P_\chi(z)\chi(t) \qquad (2)$$

where P_V and P_χ are the interpolating functions which approximate the displacements within the tower. These are conveniently represented as cubic polynomials satisfying the necessary boundary conditions of a cantilever tower. Using this expression for the tower bending displacement, the stiffness and mass coefficients may be obtained by one of the numerous energy methods. In terms of the interpolating functions P_V and P_χ, the generalized stiffness and mass coefficients for the tower may be expressed as

$$k_{ij} = \int_0^L EI(z)P_i''(z)P_j''(z)dz \qquad (3)$$

$$m_{ij} = \int_0^L m(z)P_i(z)P_j(z)dz \qquad (4)$$

where EI(z) and m(z) are the stiffness and mass per unit length as a function of height. For additional detail concerning this technique, the interested reader should see Clough and Penzien [2]. Although the tower properties are the same in both bending directions, only one degree of freedom was desired for the x direction and therefore rotation of the nacelle about the rotor spin axis was neglected. The method of static condensation was used to eliminate the unwanted degree of freedom and obtain the desired x direction stiffness and inertia coefficients as

$$k_{UU} = k_{VV} = k^2_{V\chi}/k_{\chi\chi} \qquad (5)$$

$$m_{UU} = m_{VV} - 2(k_{V\chi}/k_{\chi\chi})m_{V\chi} + (k_{V\chi}/k_{\chi\chi})^2 m_{\chi\chi} \qquad (6)$$

In addition, the nacelle and rotor inertias add directly to the tower inertia coefficients, m_{ij}, to give the turbine system inertias. A detailed tabulation of the various terms in the inertia matrix is provided in the Appendix. There is also a gyroscopic coupling between the turbine

pitch and yaw motions. This coupling coefficient appears in the damping matrix and is given by

$$C_{\phi\chi} = I_r\Omega = -C_{\chi\phi} \tag{7}$$

where I_r is the total effective inertia of all the spinning mass connected to the turbine rotor. Using this simple model the structural stiffness and inertia coefficients for a particular wind turbine are numerically calculated using a TI-59 calculator code [3].

Aerodynamic Forces

The geometry of the three-bladed rigid rotor is illustrated in Figure 2. The blades are coned at an angle β_0, and are assumed to be twisted and tapered. The angle θ defines the pitch setting as the angle from the plane of rotation to the zero-lift-line of the airfoil at the blade tip.

For this analysis, quasi-static aerodynamics will be used to compute the forces acting on the blades due to the turbulent wind and structural motion. The wind input including turbulence is assumed to be made up of a steady mean wind, V_w, plus fluctuating components, $V_i(t)$, which at any instant are constant over the rotor disk and turbulence gradients $V_{i,j}(t)$, which vary linearly across the disk. Both $V_i(t)$ and $V_{i,j}(t)$ may be thought as disk averaged time dependent quantities. This allows the wind velocity to be written in a linear expansion as

$$\{V_\infty\} = \begin{Bmatrix} 0 \\ V_w \\ 0 \end{Bmatrix} + \begin{Bmatrix} V_x \\ V_y \\ V_z \end{Bmatrix} + \begin{bmatrix} V_{x,x} & V_{x,y} & V_{x,z} \\ V_{y,x} & V_{y,y} & V_{y,z} \\ V_{z,x} & V_{z,y} & V_{z,z} \end{bmatrix} \begin{Bmatrix} r\sin\Omega t \\ 0 \\ r\cos\Omega t \end{Bmatrix} \tag{8}$$

where r is the radial position in the rotor disk, and Ωt is the azimuthal location. Motivation for this particular form for the turbulence and discussion of its accuracy is presented in the companion paper, reference [1]. In this equation the mean wind direction coincides with the y axis of Figure 2. In addition, the spatial change in the y direction turbulence component due to the coning has been dropped in the above expression, which eliminates the effect of the turbulence gradients $V_{i,y}$.

Using the above wind representation and fundamental kinematic relationships provides the relative velocity as observed from the turbine blade. The relative velocity is made up of contributions from the wind, the moving structure and the induced velocity caused by aerodynamic action. In equation form this is

$$\vec{V}_{rel} = \vec{V}_\infty - \vec{V} - \vec{v}_i \tag{9}$$

In terms of the displacement coordinates, the relative velocity components parallel and perpendicular to the rotor disk rotational plane are given by

$$\begin{aligned} V_\mu/R\Omega = {} & r\Omega/R\Omega + \{r\dot{\Psi} + \cos\Omega t[-\phi(V_w - v_i) - \delta V_x \\ & + \dot{U} - a\dot{\phi}] \\ & + \sin\Omega t[-\chi(V_w - v_i) + \delta V_z \\ & - a\dot{\chi}]\}/R\Omega \\ V_\nu/R\Omega = {} & (V_w - v_i)/R\Omega + \{\delta V_y + \cos\Omega t[-\beta_0\delta V_z + r\dot{\chi}] \\ & + \sin\Omega t[\beta_0(\dot{U} - \delta V_x) \\ & - r\dot{\phi}]\}/R\Omega \end{aligned} \tag{10}$$

where the fluctuating part of the wind turbulence has been written as δV_i to shorten the expressions. These expressions have also been linearized assuming small displacements, and wind fluctuations; however, in some places the product of the static coning angle and the wind fluctuation were retained because of interest in their effect.

Referring to Figure 3, the aerodynamic forces parallel and perpendicular to the rotor plane may be written as

$$\begin{aligned} dA_\mu &= \tfrac{1}{2}\rho a' c\, d\xi\{-\eta V_\mu^2 - \theta V_\nu V_\mu + (1-\eta/2)V_\nu^2\} \\ dA_\nu &= \tfrac{1}{2}\rho a' c\, d\xi\{-\theta V_\mu^2 + (1+\eta)V_\nu V_\mu - \theta V_\nu^2/2\} \end{aligned} \tag{11}$$

where the lift and drag for a blade element have been calculated using the static formulas with the instantaneous velocities. In the above expressions a' is the slope of the sectional lift curve $dC_L/d\alpha$, c is the local airfoil chord, η is the ratio C_{D_0}/a', and ρ is the air density.

Using the wind input of Eq. (8), together with the velocity expressions of Eq. (10) and substituting into the aerodynamic force relationships gives

$$\begin{aligned} dA_\mu = {} & \tfrac{1}{2}\rho a' c_t (R\Omega)^2 R\,dx\{A' - B'[f_0 + f_c\cos\Omega t + f_s\sin\Omega t \\ & + f_{c2}\cos 2\Omega t + f_{s2}\sin 2\Omega t] \\ & + C'[g_0 + g_c\cos\Omega t + g_s\sin\Omega t \\ & + g_{c2}\cos 2\Omega t + g_{s2}\sin 2\Omega t]\} \\ dA_\nu = {} & \tfrac{1}{2}\rho a' c_t (R\Omega)^2 R\,dx\{D' + E'[f_0 + f_c\cos\Omega t + f_s\sin\Omega t \\ & + f_{c2}\cos 2\Omega t + f_{s2}\sin 2\Omega t] \\ & + F'[g_0 + g_c\cos\Omega t + g_s\sin\Omega t \\ & + g_{c2}\cos 2\Omega t + g_{s2}\sin 2\Omega t]\} \end{aligned} \tag{12}$$

where the primed quantities are the aerodynamic constants

$$\begin{aligned} A'(x) &= [(1-\eta/2)\lambda^2 - x(\eta x + \theta\lambda)]c/c_t \\ B'(x) &= [2\eta x + \theta\lambda]c/c_t \qquad C'(x) = [(2-\eta)\lambda - \theta x]c/c_t \\ D'(x) &= [(1+\eta)\lambda x - \theta(x^2 + \lambda^2/2)]c/c_t \\ E'(x) &= [(1+\eta)\lambda - 2\theta x]c/c_t \\ F'(x) &= [(1+\eta)x - \lambda\theta]c/c_t \end{aligned} \tag{13}$$

with $x = r/R = (h+\xi)/R$, $\lambda = (V_w - v_i)/R\Omega$, and c_t is the chord at the rotor tip. Note that both the pitch setting, θ, and the blade chord, c, may be functions of x. In the above force equations the

subscripted f and g variables are combinations of the wind inputs and response variables and are defined as follows:

$$
\begin{aligned}
f_0 &= r(\dot{\Psi} + \gamma_{zx})/R\Omega \\
f_c &= -\phi\lambda+(-V_x + \dot{U} - a\dot{\phi})/R\Omega \\
f_s &= -\chi\lambda+(V_z - a\dot{\chi})/R\Omega \\
f_{c2} &= -r\,\bar{\gamma}_{zx}/R\Omega \\
f_{s2} &= r\bar{\varepsilon}_{zx}/R\Omega \\
\gamma_{zx} &= \frac{1}{2}(V_{z,x} - V_{x,z}) \\
\varepsilon_{zx} &= \frac{1}{2}(V_{z,z} - V_{x,x}) \\
g_0 &= (V_y - \dot{V} - r\beta_0\bar{\varepsilon}_{zx})/R\Omega \\
g_c &= (r\dot{\chi} + rV_{y,z} - \beta_0 V_z)/R\Omega \\
g_s &= (\beta_0(\dot{U} - V_x) - r\dot{\phi} + rV_{y,x})/R\Omega \\
g_{c2} &= -\beta_0 f_{s2} \\
g_{s2} &= \beta_0 f_{c2} \\
\bar{\gamma}_{zx} &= \frac{1}{2}(V_{z,x} + V_{x,z}) \\
\bar{\varepsilon}_{zx} &= \frac{1}{2}(V_{z,z} + V_{x,x})
\end{aligned}
\qquad (14)
$$

To obtain the aerodynamic coefficients for the total forces acting on the rotor hub, the appropriate components of the blade element forces, Eq. (12), are summed over the three blades and integrated with respect to radius for a specified induced velocity distribution. This gives the net thrust, torque, horizontal and vertical forces, and the yaw and pitch moments, which are to be added to the structural terms resulting in the final equations of motion, Eq. (1). A detailed list of these equations is provided in the Appendix.

The Induced Velocity

The aerodynamics of wind turbines involve highly complex flow phenomena, which require rather sophisticated theories in order to obtain accurate predictions. However, some fairly simple theories making relatively crude assumptions can often give reasonable estimates and generally can give excellent insight into the physical phenomena of interest. In this case two different wake models were used in an effort to gain insight into the significance of changes in the induced velocity field on wind turbine response to turbulence.

For the first wake model, the induced velocity was computed using blade element theory following the approach of Wilson [4], and performing a momentum balance neglecting wake rotation. This provided the induced velocity as a function of radius, under the assumption that the rotor axis was perfectly aligned with the wind direction. After the induced velocity distribution was computed for a given mean operating condition, it was assumed to be constant and independent of turbulent wind fluctuations. This model was named the "frozen wake model."

The second wake model was called the "equilibrium wake." For this model, the axial fluctuations in wind velocity are assumed to occur so slowly that the induced velocity is the steady state value for the instantaneous wind speed. In this situation, the axial flow will be not only time varying but nonuniform, because of the inclusion of the fluctuating wind gradient terms in the turbulence model of Eq. (8). These gradients could be thought of as slowly changing wind shears of arbitrary orientation, since their effect on the wind turbine would be similar. To obtain an approximation for the induced velocities of this "equilibrium wake," the "semi-rigid" wake model discussed by Miller [5] was used. Miller shows that the effect of including the induced velocity due to the nonuniform flow is to reduce the lift by a factor referrred to as the "lift deficiency" function.

For this analysis, assuming small velocity changes, the lift deficiency function was approximately

$$
\mathcal{L}_{d(x)} = \frac{1}{1+\tau_t F'(x)/x(2\lambda-\lambda_w)} \qquad (15)
$$

where $\lambda_w = V_w/R\Omega$ and $\tau_t = 3a'c_t/8\pi R$. In addition, the azimuthal change in the induced velocity distribution led to a change in the in-plane aerodynamic coefficients B'(x), where the change was

$$
\Delta B'(x) = \tau_t[B'(x)F'(x)+C'(x)E'(x)]/\{x(2\lambda-\lambda_w)\} \qquad (16)
$$

Because this change is small, it was tempting to neglect it, but all of the in-plane forces are small so it was retained. Finally, the wind fluctuations in the axial direction V_y, $V_{y,z}$ and $V_{y,x}$ are associated with a change in momentum in the streamwise direction which, for the assumptions of this wake model, change the equilibrium thrust. This added lift factor is approximately

$$
\mathcal{L}_a(x) = 1 + \lambda/(2\lambda-\lambda_w) \qquad (17)
$$

To incorporate these effects, the aerodynamic coefficients B'(x), C'(x), E'(x) and F'(x) of Eq. (13) were modified in the following manner to obtain the "equilibrium wake" coefficients:

$$
\begin{aligned}
B'_e(x) &= \mathcal{L}_d(x)\{B'(x)+\Delta B'(x)\} \\
C'_e(x) &= \mathcal{L}_d(x)C'(x) \\
E'_e(x) &= \mathcal{L}_d(x)E'(x) \\
F'_e(x) &= \mathcal{L}_d(x)E'(x) \\
C'_{ey}(x) &= \mathcal{L}_d(x)\mathcal{L}_a(x)C'(x) \\
F'_{ey}(x) &= \mathcal{L}_d(x)\mathcal{L}_a(x)C'(x)
\end{aligned}
\qquad (18)
$$

where the two coefficients C'_{ey} and F'_{ey} are specifically associated with the wind fluctuations V_y, $V_{y,z}$ and $V_{y,x}$. The aerodynamic coefficients A'(x) and D'(x) are related to the mean thrust and torque and are thus unaffected by wind fluctuations. Computationally, the influence of the wake model can be observed by changing the primed aerodynamic coefficients in the blade element force relationships Eq. (12).

Although both of these wake models were useful in developing an understanding of the influence of the induced velocity distribution on machine response to turbulence, it is unclear whether either model accurately approximates the real distributions and future work is needed to evaluate the effects of unsteady wake aerodynamics.

State Space Equations

The equations of motion Eq. (1) can be written in matrix form

$$[M]\{\ddot{X}\}+[C]\{\dot{X}\}+[K]\{X\} = \{Q_1\}+[F]\{u\} \qquad (19)$$

where

$$\{X\}^T = (U,V,\phi,\chi,\Psi) = \text{displacement coordinate}$$

$$\{Q_1\}^T = (0,T,0,Q,0) = \text{steady state}$$

$$\{u\}^T = (V_x,V_y,V_z,V_{y,x},V_{y,z},\gamma_{xz},\varepsilon_r,\bar{\gamma}_r,\bar{\varepsilon}_{xz}) = \text{wind inputs}$$

$$\varepsilon_r = \varepsilon_{zx}\cos 3\Omega t + \bar{\gamma}_{zx}\sin 3\Omega t$$

$$\bar{\gamma}_r = -\varepsilon_{zx}\sin 3\Omega t + \bar{\gamma}_{zx}\cos 3\Omega t$$

Furthermore, it is possible to model each of the nine turbulence inputs using a set of stochastic differential equations of the form

$$\{\dot{u}\} = [A_w]\{u\} + [B_w]\{w\} \qquad (20)$$

where the components of {w} are white noise of equal power spectral density, $[B_w]$ is the white noise input distribution matrix which is diagonal. The $[A_w]$ matrix is diagonal except for two elements

$$[A_w] = \begin{bmatrix} a_{11} & & & & \\ & \ddots & & & \\ & & a_{77} & 3\Omega & \\ & & -3\Omega & a_{88} & \\ & & & & a_{99} \end{bmatrix}$$

which arise as a result of the $\sin 3\Omega t$ and $\cos 3\Omega t$ in the ε_r and $\bar{\gamma}_r$ wind inputs. A more detailed presentation of the wind input model is presented in the companion paper [1].

Discarding the steady terms, it is convenient to transform the equations of motion given in Eq. (19) to the state space form, so that they are written as a set of first order equations similar to the turbulence inputs of Eq. (20). To further facilitate the computation of results, the state space form of Eq. (19) can be augmented with the turbulence inputs, Eq. (20), to form a single system of equations with white noise as the driving input. The five turbine displacements and their derivatives together with the nine turbulence inputs will form the state vector for this augmented system. The governing equations can then be written

$$\{\dot{x}\} = [A]\{x\} + [B]\{w\}$$

$$\{y\} = [c]\{x\} \qquad (21)$$

where

$$\{x\} = \begin{Bmatrix} \{X\} \\ \{\dot{X}\} \\ \{u\} \end{Bmatrix} \qquad [A] = \begin{bmatrix} [0] & [I] & [0] \\ -[M]^{-1}[K] & -[M]^{-1}[K] & [M]^{-1}[F] \\ [0] & [0] & [A_w] \end{bmatrix}$$

$$[B] = \begin{bmatrix} [0] \\ [B_w] \end{bmatrix} \qquad \{y\} = \begin{Bmatrix} F_x \\ F_y \\ M_z \\ M_x \\ \text{Power} \\ \{x\} \end{Bmatrix} = \text{outputs}$$

$$[c] = \begin{bmatrix} [K] & [0] \\ (00\ldots\Omega c_g\ldots 0) & \\ [0] & [I] \end{bmatrix} = \text{response matrix}$$

With this formulation it is a relatively straightforward numerical procedure, to determine the complex eigenvalues of the A matrix and then to compute the modal matrix, which is made up of the associated eigenvectors. The modal matrix can then be used to decouple the equations of motion, so that transfer functions between any of the nine white noise inputs and any output, y_i, may be easily computed. These transfer functions account for differences in the energy level for the turbulence inputs, {u}, so that a comparison of the transfer function magnitudes provides a direct estimate of relative importance. The final result uses the central equation from random vibration theory, which states that the spectral density for any of the outputs {y} will be given by

$$\{S_y(\omega)\} = [|H_{yw}(\omega)|^2]\ \{S_w(\omega)\}$$

for uncorrelated inputs, where $\{S_y(\omega)\}$ is the spectral density of the outputs {y}, $[|H_{yw}(\omega)|^2]$ is the matrix of the transfer functions magnitude squared and $\{S_w(\omega)\}$ is the spectral density of the white noise driving inputs, which are all equal.

Results

To determine the influence of the turbulence inputs modeled in this work two wind systems of vastly different size were examined. The smaller machine, called the Mod-M, was an 8 kW turbine, with a three bladed rotor located downwind of the tower, and designed for free-yaw operation. The specific characteristics are as follows:

Mod-M

Rotor Characteristics:

Rotor Radius	16.67 ft
Blade Chord (constant)	1.5 ft
Coning Angle	3.5°
Blade Twist	0.0°

System Frequencies:

1st Bending (fore-aft)	15.1 rad/s
2nd Bending (fore-aft)	53.1 rad/s
1st Side to Side	15.9 rad/s

Aerodynamic Properties:

Lift Curve Slope	5.7
Drag Coefficient, C_{D_0}	.02
Stall not Modeled	

Operating Conditions Used:

Wind Velocity (mean)	16.63 MPH
Rotor Speed (mean)	73.35 RPM
Pitch Setting (to ZLL)	3.0°
Turbulence Length Scale	300 ft
Rms Turbulent Intensity	2.03 ft/s
Approximate Output	6 kW

Selected analysis results for this situation are shown in the power spectral density plots of Figures 4 through 6. The figures clearly illustrate the difference in response for the two wake models. For forces and moments which are highly dependent on the streamwise velocity such as thrust, the equilibrium wake assumptions give a larger response, as shown in Figure 4. This figure also indicates a significant response at the two system fore-aft bending frequencies. Figure 5 shows the yaw response, while Figure 6 gives the pitching moment response. These two figures indicate the degree of coupling between pitch and yaw for this free-yaw turbine. Notice that as the yaw response increases, there is a corresponding increase in the pitching moment. Figure 6 also shows a small response peak at 3Ω, which is the result of the $\sin 3\Omega t$ and $\cos 3\Omega t$ in the ε_r and $\bar{\gamma}_r$ inputs.

The second wind system to be analyzed in this study was a large turbine called the Mod-G. The Mod-G was 2.5 MW turbine with a three bladed rotor located upwind of the tower, and was designed for fixed-yaw operation. The specific characteristics of this system are:

Mod-G

Rotor Characteristics:

Rotor Radius	150 ft
Blade Chord (linear taper)	7.74 ft at hub to 3.15 ft at tip
Coning Angle	4°
Blade Twist (linear)	8°

System Frequencies:

1st Bending (fore-aft)	2.75 rad/s
2nd Bending (fore-aft)	12.8 rad/s
1st Side to Side	2.9 rad/s
2nd Side to Side	9.5 rad/s

Aerodynamic Properties:

Lift Curve Slope	5.73
Drag Coefficient, C_{D_0}	.008
Stall not Modeled	

Operating Conditions:

Wind Velocity	20 MPH
Rotor Speed	17.5 RPM
Pitch Setting at tip	-6.2°
Turbulence Length Scale	500 ft
Rms turbulent intensity	2.44 ft/s
Approximate Power Output	1.1 MW

Figures 7, 8 and 9 shows some typical results for the Mod-G. As was the case in the previous plots, the system frequencies are easily identified.

The primary objective of this work was to identify the features of turbulence which are most important in wind turbine design. In an effort to focus on these key features, the response at specific system frequencies was broken down into fractional contributions from each turbulence input. The most significant results of these calculations are tabulated in Tables 1 and 2.

From these results it would appear that the most important inputs are the three longitudinal turbulence terms, and in some instances, the two in-plane shear terms which have an effective frequency of 3Ω. An alternate means of presenting this same information is to plot power spectral density curves for the various outputs using only the turbulence input V_y, and then adding the two gradients $V_{y,x}$ and $V_{y,z}$. This has been done in Figures 10 through 15 for the outputs previously presented. As can be seen from these figures, a major contribution to the machine excitation is lost if the turbulence gradients are not included. However, neglecting the $\bar{\gamma}_r$ and ε_r appears to have only a local influence around the frequency 3Ω.

Conclusions and Recommendations

On the basis of the work done in this study, the longitudinal turbulence input, V_y, and the two gradients, $V_{y,x}$ and $V_{y,z}$ are of equal importance when computing the dynamic response of wind systems, and these three inputs together comprise the major excitation source for horizontal axis wind turbines. Because of the simplifying assumptions and approximations used in this analysis, it is imperative that the results and the technique be validated with experimental data, prior to use for design.

ACKNOWLEDGEMENTS

This research was supported by the Department of Energy through Battelle, Pacific Northwest Laboratory, under Contract DE-AT06-79ET23144. The authors would particularly like to thank Dr. J.R. Connell, the technical monitor, for his enthusiastic support, and the many valuable suggestions made by the PNL staff. The responsibility for the results and the opinions expressed rests with the authors and not the United States Government or Oregon State University.

REFERENCES

1. Holley, W.E., "Wind Turbulence Inputs for Horizontal Axis Wind Turbines," Second DOE/NASA Wind Turbine Dynamics Workshop, February 1981.

2. Clough, R.W. and Penzien, J., Dynamics of Structures, McGraw-Hill, 1975.

3. Jafarey, N., and Thresher, R., "Turbine System Natural Frequencies," Program Record for TI-59 Programmable Calculator, Program Records No. 101 and 102, Mech. Engrng. Dept., Oregon State University.

4. Wilson, R.E., and Lissaman, P.B.S., Applied Aerodynamics of Wind Power Machines, Oregon State University Report, NTIS PB-238-595, 1974.

5. Miller, R., Dugundji, J., Martinez-Sanchez, M., Gohard, J., Chung, S., and Humes, T, Aerodynamics of Horizontal Axis Wind Turbines, Volume II of Wind Energy Conversion, Report ASRL TR-184-8, Dept. of Aeronautics and Astronautics, MIT, Sept. 1978.

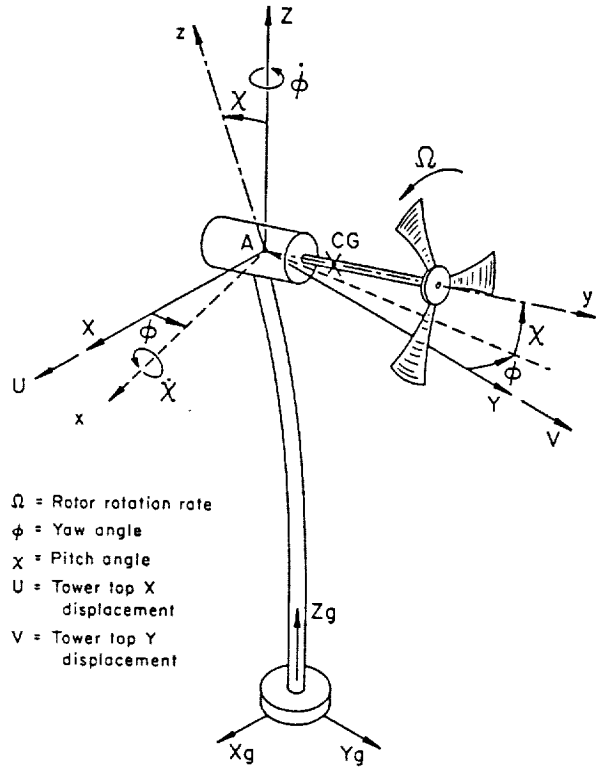

FIGURE 1. THE TURBINE MODEL.

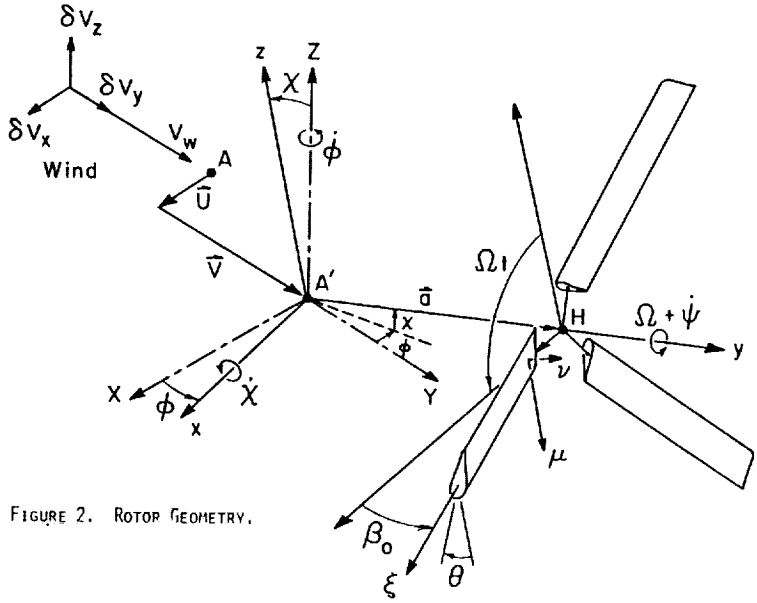

FIGURE 2. ROTOR GEOMETRY.

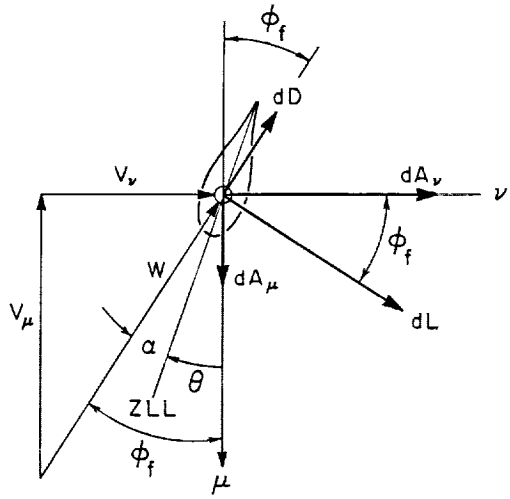

FIGURE 3. BLADE ELEMENT AERODYNAMIC FORCES.

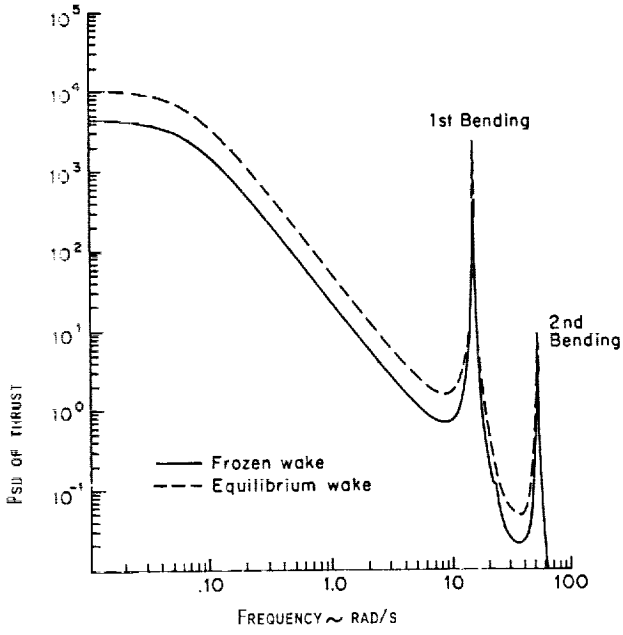

FIGURE 4. MOD-M POWER SPECTRAL DENSITY PLOT OF THRUST, F_Y.

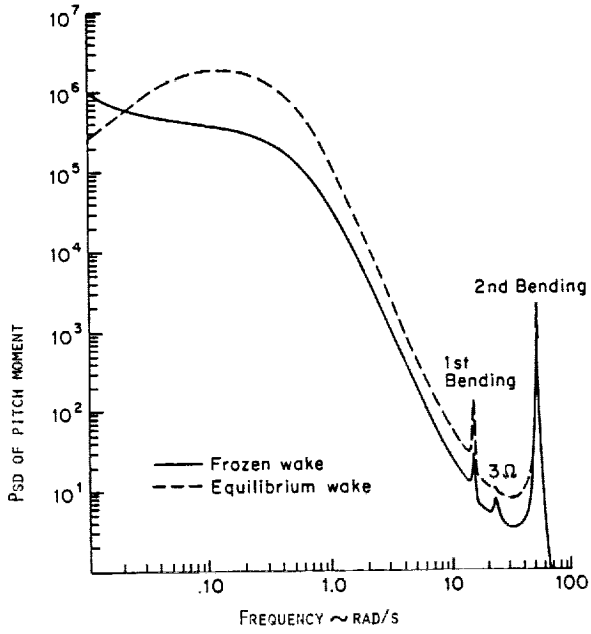

FIGURE 6. MOD-M POWER SPECTRAL DENSITY OF PITCH MOMENT, M_X.

ERRATUM: The power spectral densities shown in Figures 4-15 are incorrectly plotted. The ordinate, Psd, should be increased by exactly a factor of 10 to be correct.

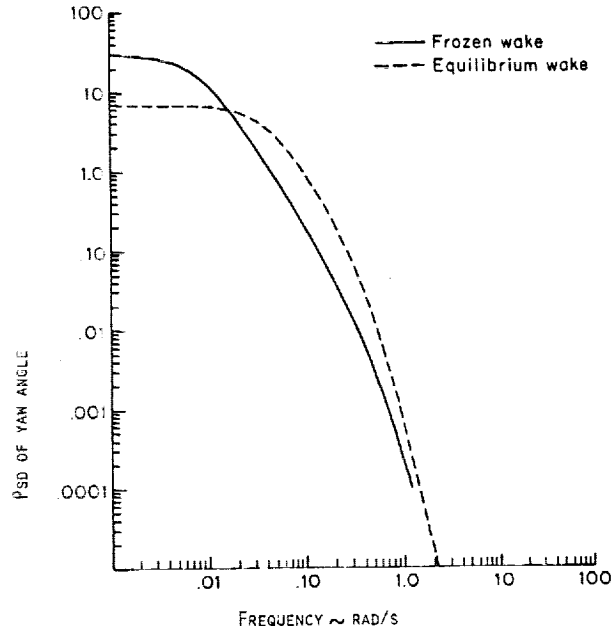

FIGURE 5. MOD-M POWER SPECTRAL DENSITY OF YAW ANGLE, ø.

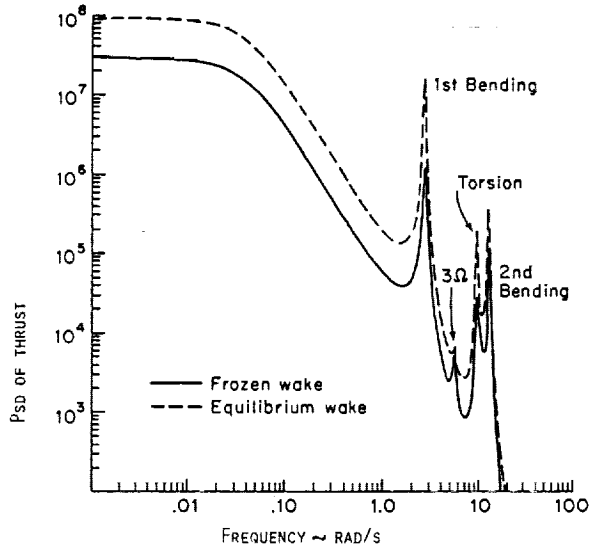

FIGURE 7. MOD-G POWER SPECTRAL DENSITY OF THRUST, F_Y.

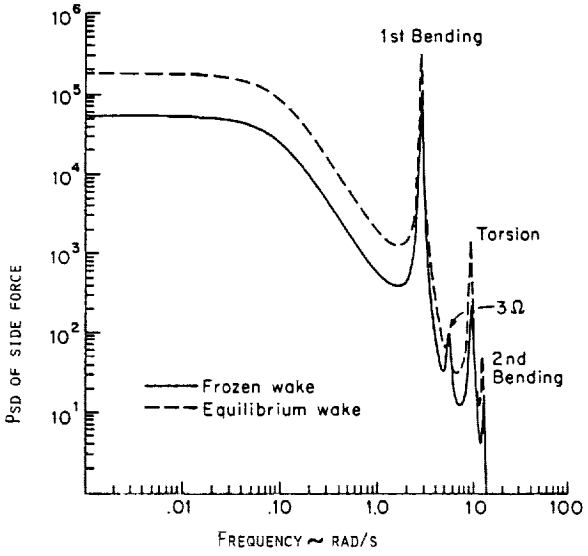

FIGURE 8. MOD-G POWER SPECTRAL DENSITY OF SIDE FORCE, F_x.

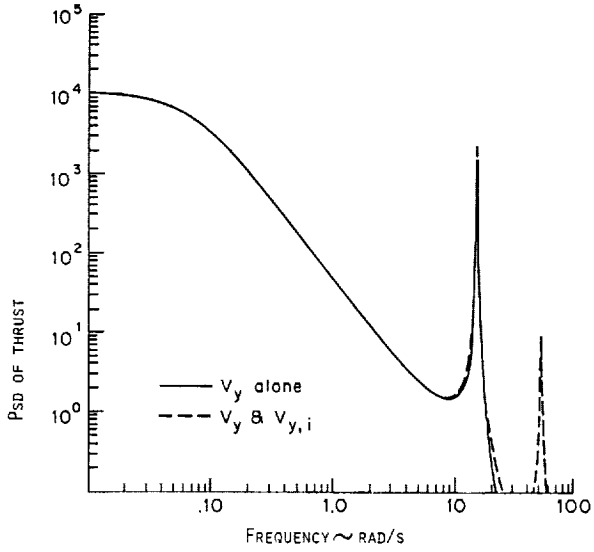

FIGURE 10. THE EFFECT OF THE GRADIENTS $V_{Y,X}$ & $V_{Y,Z}$ ON THRUST FOR MOD-M USING THE EQUILIBRIUM WAKE.

ERRATUM: The power spectral densities shown in Figures 4-15 are incorrectly plotted. The ordinate, Psd, should be increased by exactly a factor of 10 to be correct.

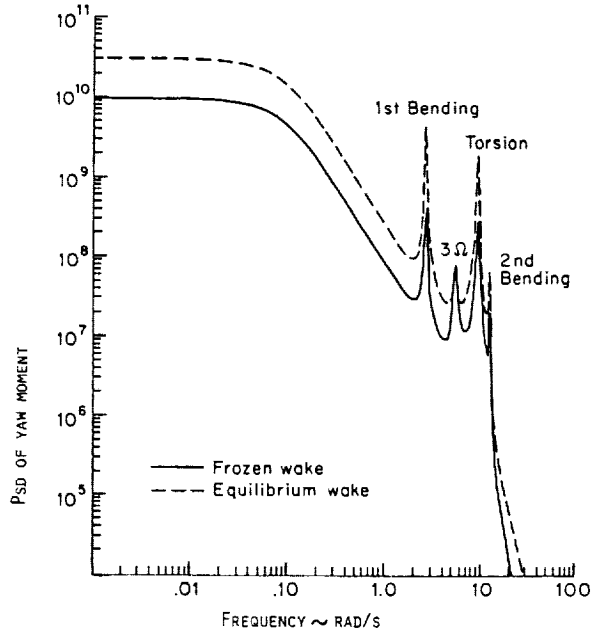

FIGURE 9. MOD-G POWER SPECTRAL DENSITY OF YAW MOMENT, M_z.

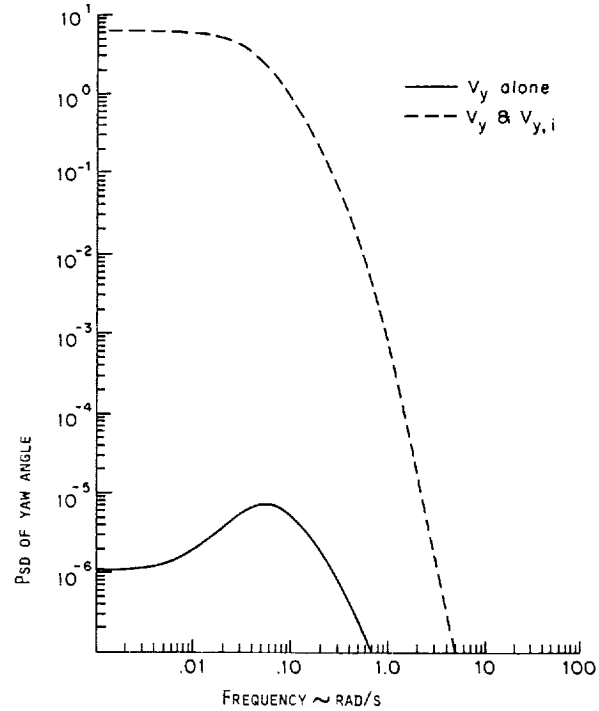

FIGURE 11. THE EFFECT OF THE GRADIENTS $V_{Y,X}$ & $V_{Y,Z}$ ON YAW ANGLE FOR MOD-M USING THE EQUILIBRIUM WAKE.

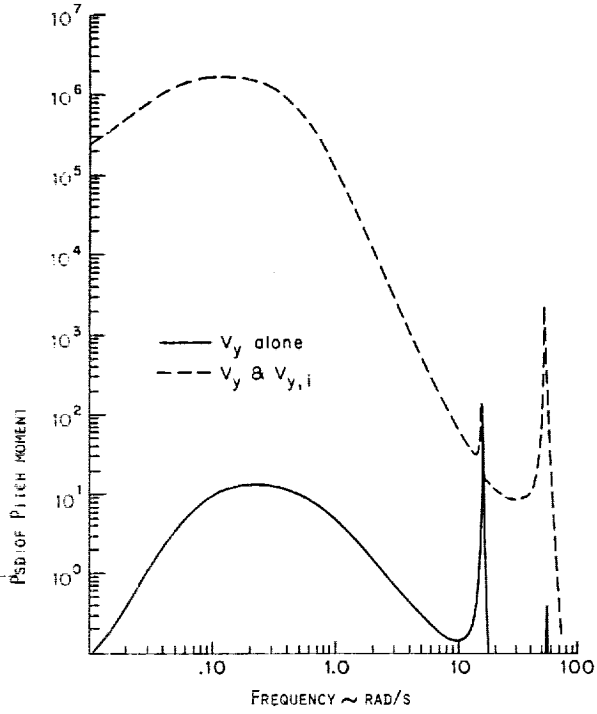

FIGURE 12. THE EFFECT OF THE GRADIENTS $V_{Y,X}$ & $V_{Y,Z}$ ON PITCH MOMENT FOR MOD-M USING THE EQUILIBRIUM WAKE.

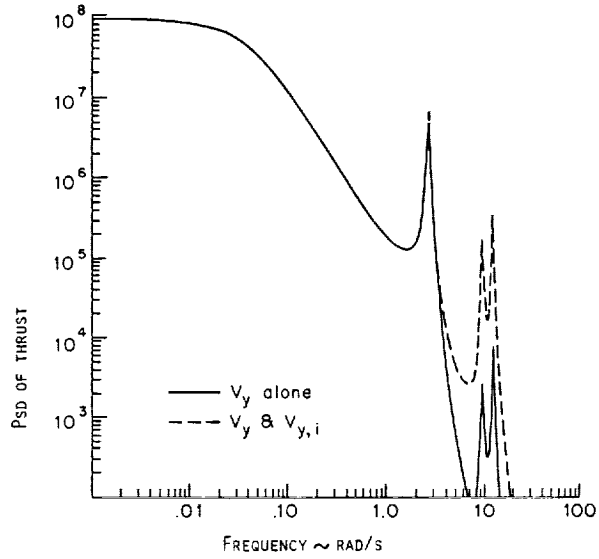

FIGURE 14. THE EFFECT OF THE TURBULENCE GRADIENTS $V_{Y,X}$ & $V_{Y,Z}$ ON THE THRUST FOR THE MOD-G USING THE EQUILIBRIUM WAKE.

ERRATUM: The power spectral densities shown in Figures 4-15 are incorrectly plotted. The ordinate, Psd, should be increased by exactly a factor of 10 to be correct.

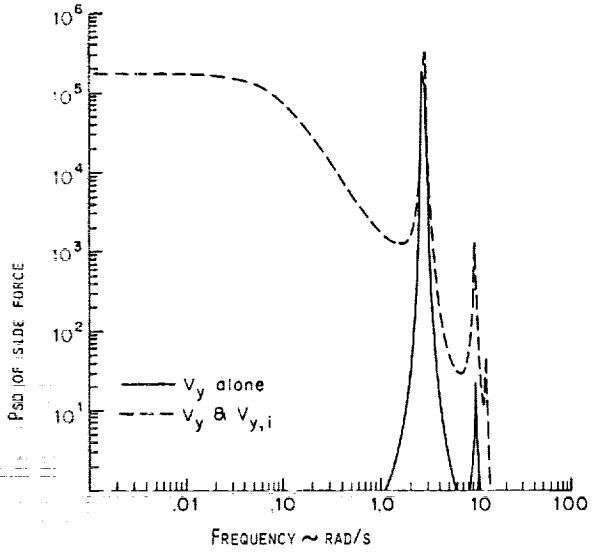

FIGURE 13. THE EFFECT OF THE GRADIENTS $V_{Y,X}$ & $V_{Y,Z}$ ON SIDE FORCE FOR THE MOD-G USING THE EQUILIBRIUM WAKE.

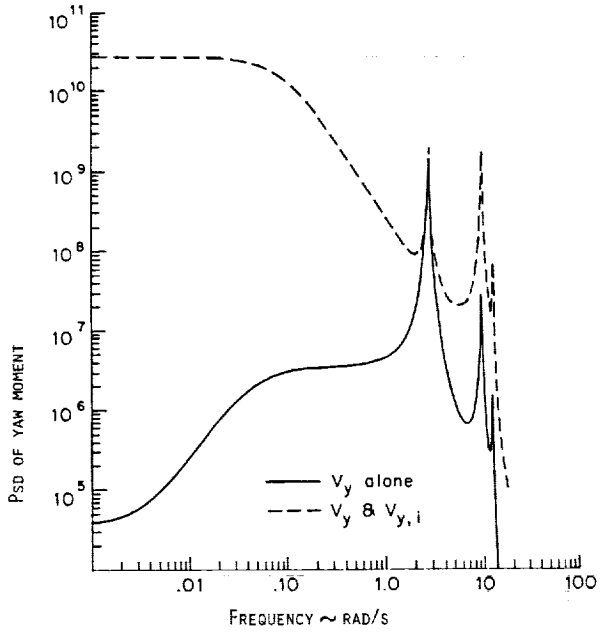

FIGURE 15. THE EFFECT OF THE GRADIENTS $V_{Y,X}$ & $V_{Y,Z}$ ON YAW MOMENTS FOR THE MOD-G USING THE EQUILIBRIUM WAKE.

Table 1. Fractional response contributions of the turbulence inputs for the Mod-M using the equilibrium wake.

Response/Input	V_y	$V_{y,x}$	$V_{y,z}$	ϵ_r	$\bar{\gamma}_r$	Other
Frequency ≃ 0						
Side Force, F_x	.0	.96	.0	.0	.0	.04
Thrust, F_y	1.0	.0	.0	.0	.0	.0
Pitch Moment, M_x	.0	.82	.12	.0	.0	.06
Frequency = 15.1 (1st Bending)						
Side Force, F_x	.33	.07	.56	.0	.0	.04
Thrust, F_y	.75	.06	.18	.0	.0	.01
Pitch Moment, M_x	.70	.07	.22	.0	.0	.01
Frequency = 3Ω = 23						
Side Force, F_x	.0	.02	.69	.14	.13	.02
Thrust, F_y	.32	.08	.52	.04	.04	.0
Pitch Moment, M_x	.0	.11	.77	.06	.06	.0

Table 2. Fractional response contributions of the turbulence inputs for the Mod-G using the equilibrium wake.

Response/Input	V_y	$V_{y,x}$	$V_{y,z}$	ϵ_r	$\bar{\gamma}_r$	Other
Frequency ≃ 0						
Side Force, F_x	.0	.06	.92	.0	.0	.02
Thrust, F_y	1.0	.0	.0	.0	.0	.0
Yaw Moment, M_z	.0	.97	.0	.0	.0	.03
Pitch Moment, M_x	.0	.0	.97	.0	.0	.0
Frequency = 2.76 (1st Bending)						
Side Force, F_x	.90	.02	.07	.0	.0	.01
Thrust, F_y	.77	.0	.22	.0	.0	.01
Yaw Moment, M_z	.77	.01	.21	.0	.0	.01
Pitch Moment, M_x	.76	.0	.23	.0	.0	.01
Frequency = 3Ω = 5.5						
Side Force, F_x	.01	.36	.07	.27	.27	.02
Thrust, F_y	.06	.05	.42	.22	.24	.01
Yaw Moment, M_z	.01	.29	.0	.35	.34	.01
Pitch Moment, M_x	.0	.05	.45	.23	.25	.02

APPENDIX

Governing Equations:

$$\begin{bmatrix} M_{11} & 0 & M_{13} & 0 & 0 \\ 0 & M_{22} & 0 & M_{24} & 0 \\ M_{31} & 0 & M_{33} & 0 & 0 \\ 0 & M_{42} & 0 & M_{44} & 0 \\ 0 & 0 & 0 & 0 & M_{55} \end{bmatrix} \begin{Bmatrix} \ddot{U} \\ \ddot{V} \\ \ddot{\phi} \\ \ddot{\chi} \\ \ddot{\psi} \end{Bmatrix} + \begin{bmatrix} C_{11} & 0 & C_{13} & C_{14} & 0 \\ 0 & C_{22} & 0 & 0 & C_{25} \\ C_{31} & 0 & C_{33} & C_{34} & 0 \\ C_{41} & 0 & C_{43} & C_{44} & 0 \\ 0 & C_{52} & 0 & 0 & C_{55} \end{bmatrix} \begin{Bmatrix} \dot{U} \\ \dot{V} \\ \dot{\phi} \\ \dot{\chi} \\ \dot{\psi} \end{Bmatrix} + \begin{bmatrix} K_{11} & 0 & K_{13} & K_{14} & 0 \\ 0 & K_{22} & 0 & K_{24} & 0 \\ 0 & 0 & K_{33} & K_{34} & 0 \\ 0 & K_{42} & K_{43} & K_{44} & 0 \\ 0 & 0 & 0 & 0 & 0 \end{bmatrix} \begin{Bmatrix} U \\ V \\ \phi \\ \chi \\ \psi \end{Bmatrix}$$

$$= \begin{Bmatrix} 0 \\ T \\ 0 \\ 0 \\ Q \end{Bmatrix} + \begin{bmatrix} F_{11} & 0 & F_{13} & F_{14} & F_{15} & 0 & F_{17} & F_{18} & 0 \\ 0 & F_{22} & 0 & 0 & 0 & F_{26} & 0 & 0 & F_{29} \\ F_{31} & 0 & F_{33} & F_{34} & F_{35} & 0 & F_{37} & F_{38} & 0 \\ F_{41} & 0 & F_{43} & F_{44} & F_{45} & 0 & F_{47} & F_{48} & 0 \\ 0 & F_{52} & 0 & 0 & 0 & F_{56} & 0 & 0 & F_{59} \end{bmatrix} \begin{Bmatrix} V_x \\ V_y \\ V_z \\ V_{y,x} \\ V_{y,z} \\ \gamma_{zx} \\ (\varepsilon_{zx}\cos 3\Omega t + \bar{\gamma}_{zx}\sin 3\Omega t) \\ (-\varepsilon_{zx}\sin 3\Omega t + \bar{\gamma}_{zx}\cos 3\Omega t) \\ \bar{\varepsilon}_{zx} \end{Bmatrix}$$

Inertia Matrix

$M_{11} = m_{11} + m_n + m_r$; $M_{13} = M_{31} = -(m_n + m_r)q$

$M_{22} = m_{22} + m_r + m_n$; $M_{24} = m_{24} = M_{42}$; $M_{33} = m_{33} + I_{zz}$

$M_{44} = m_{44} + I_{xx}$; $M_{55} = I_r$; m_r = mass of rotor ; m_n = mass of nacelle

q = distance from C_L tower to nacelle-rotor C.G. ; I_{xx} and I_{yy} = mass moment of inertia of nacelle-rotor system about x and y axes ; I_r = rotor effective spinning inertia ; m_{ij} = tower inertia coefficients of Eq. (4), where for a uniform cantilever tower,

$m_{11} = 99\, m_t/420$, $m_{22} = 156\, m_t/420$, $m_{24} = 22\, m_t L/420$

$m_{33} = I_m L/3$, $m_{44} = m_t L^2/105$, m_t = tower mass , I_m = tower polar inertia

Damping Matrix

$C_{11} = 3f(B_o+\beta_o^2 F_o)/2R\Omega$; $C_{13} = -3f(\bar{a}B_o+\beta_o F_1)/2\Omega$; $C_{14} = -3f(C_1+\bar{a}\beta_o E_o)/2\Omega$

$C_{22} = 3fF_o/R\Omega$; $C_{25} = -3fE_1/\Omega$; $C_{31} = -3f(\beta_o\{F_1+B_1^*\}+\bar{a}\{B_o+\beta_o^2 F_o\})/2\Omega$

$C_{33} = 3fR(\{F_2+\beta_o\bar{a}B_1^*\}+\bar{a}\{\bar{a}B_o+\beta_o F_1\})/2\Omega$; $C_{34} = 3fR(\{E_1\bar{a}+\beta_o C_2^*\}+\bar{a}\{C_1+\bar{a}\beta_o E_o\})/2\Omega+I_r\Omega$

$C_{41} = 3f(\{E_1+\beta_o^2 C_1^*\}+\bar{a}\beta_o\{C_o+E_o\})/2\Omega$; $C_{43} = -C_{34}$; $C_{44} = C_{33}$

$C_{52} = 3fC_1/\Omega$; $C_{55} = 3fRB_2/\Omega+C_g$; C_g = Generator torque coefficient

Stiffness Matrix

$K_{11} = k_{11}$; $K_{13} = -3fG_o/2$; $K_{14} = -3f\beta_o H_o/2$; $K_{22} = k_{22}$; $K_{24} = k_{24}$

$K_{33} = k_{33} + 3fR(\beta_o G_1^*+\bar{a}G_o)/2$; $K_{34} = 3fR(H_1+\beta_o\bar{a}H_o)/2$; $K_{42} = K_{24}$

$K_{43} = -K_{34}$; $K_{44} = k_{44} + 3fR(\beta_o G_1^*+\bar{a}G_o)/2$

where k_{ij} = tower structural stiffnesses from Eq. (3), and for a uniform cantilever tower $k_{11} = 3EI/L^3$; $k_{22} = 12EI/L^3$; $k_{24} = 6EI/L^2$; $k_{33} = GJ/L$; $k_{44} = 4EI/L$

Wind Input Matrix

$F_{11} = 3f(B_0+\beta_0^2 F_0)/2R\Omega$; $F_{13} = -3f\beta_0(C_0+E_0)/2R\Omega$; $F_{14} = -3f\beta_0 F_1/2\Omega$

$F_{15} = 3fG_1/2\Omega$; $F_{17} = -3f\beta_0(C_1-E_1)/2\Omega$; $F_{18} = -3f(-B_1+\beta_0^2 F_1)/2\Omega$

$T = 3fD_0$; $F_{22} = 3fF_0/R\Omega$; $F_{26} = 3fE_1/\Omega$; $F_{29} = -3fF_1\beta_0/\Omega$

$F_{31} = -3f(\beta_0\{F_1+B_1^*\}+\bar{a}\{B_0+\beta_0^2 F_0\})/2\Omega$; $F_{33} = 3f(\{E_1+\beta_0^2 C_1^*\}+\bar{a}\beta_0\{C_0+E_0\})/2\Omega$

$F_{34} = 3fR(F_2+\beta_0\bar{a}F_1)/2\Omega$; $F_{35} = -3fR(\beta_0 C_2^*+\bar{a}C_1)/2\Omega$

$F_{37} = -3fR(\{E_2-\beta_0^2 C_2^*\}-\bar{a}\beta_0\{C_1-E_1\})/2\Omega$; $F_{38} = 3fR(\beta_0\{F_2-B_2^*\}+\bar{a}\{-B_1+\beta_0^2 F_1\})/2\Omega$

$F_{41} = F_{33}$; $F_{43} = -F_{31}$; $F_{44} = F_{35}$; $F_{45} = -F_{34}$; $F_{47} = -F_{38}$; $F_{48} = F_{37}$

$Q = 3fRA_1$; $F_{52} = 3fC_1/\Omega$; $F_{56} = -3fR\,B_2/\Omega$; $F_{59} = -3R\beta_0 C_2/\Omega$

where $f = \frac{1}{2}\rho a' R c_t (R\Omega)^2$. The single subscript capitalized coefficients A_n through H_n are integral aerodynamic coefficients of the form

$$A_n = \int_{\bar{h}}^{R} A'(x)\, x^n\, dx \qquad \text{where } n = 0,1,2$$

with A' through F' defined as given in Eq. (13) for the "frozen wake" or Eq. (18) for the "equilibrium wake". In addition, $G'(x) = \lambda B'(x)$ and $H'(x) = \lambda E'(x)$, while the coefficients with stars are $B_{\bar{n}}^* = B_n - \bar{h}B_{n-1}$, $C_{\bar{n}}^* = C_n - \bar{h}C_{n-1}$ and $G_{\bar{n}}^* = G_n - \bar{h}G_{n-1}$, and $\bar{h} = h/R$, $\bar{a} = a/R$.

QUESTIONS AND ANSWERS

R.W. Thresher

From: B.J. Young

Q: Your results show a substantial excitation which is continuous down through zero frequency, while J.P. Sullivan's results were zero at zero frequency. Any comment on differences?

A: *Professor Sullivan used the Davenport model for the horizontal component of wind turbulence which vanishes at zero frequency. We used the model suggested by Von Karman which is finite at zero frequency; therefore, this excitation difference at low frequency is due to the turbulence models.*

From: K.H. Hohenemser

Q: How should you expect the results to change for hinged (teetering) blades?

A: *I have not done the analysis, so I do not know exactly. I would expect the magnitude of the forces and moments to decrease significantly.*

From: Anonymous

Q: What is the effect of damping on the first and second blade bending power spectra spikes?

A: *The blade is rigid so there are no blade resonances. The bending resonances illustrated in the plots are for the tower. The only damping in the model is aerodynamic damping, but if structural damping were added, the response near resonance points should be reduced.*

From: R. E. Wilson

Q: Do you plan to treat teetering rotors?

A: *I would like to add teetering to the model, but at this time, our sponsor has not indicated a strong interest in adding this additional degree of freedom. Perhaps after the model is validated this will be possible.*